Science Advances

AAAS

advances.sciencemag.org/cgi/content/full/3/6/e1700071/DC1

Supplementary Materials for

Self-organization of maze-like structures via guided wrinkling

Hyung Jong Bae, Sangwook Bae, Jinsik Yoon, Cheolheon Park, Kibeom Kim,
Sunghoon Kwon, Wook Park

Published 30 June 2017, *Sci. Adv.* **3**, e1700071 (2017)
DOI: 10.1126/sciadv.1700071

The PDF file includes:

Other Supplementary Material for this manuscript includes the following:
(available at advances.sciencemag.org/cgi/content/full/3/6/e1700071/DC1)

- movie S1 (.avi format). Generation of the guided wrinkles.

Supplementary Materials

Formation of orthogonal ridge structures

The development of ridges and the determination of the ridge type seem to start at the ridge decision points in the first dried region and propagate to the neighboring region by satisfying boundary conditions of the ridge shape (see movie S1). The fabricated orthogonal patterns (fig. S1A) possessed a larger number of bend points than other types of points (fig. S1D). This was because the formation of the ridges in random directions was more favorable in terms of energy minimization than that of straight, bifurcation, or ending ridge types, with the designed guiding structure dimension under the isotropic shrinking process. In addition to the ending, bend, straight line, and bifurcation types, other ridge types, such as an island (an isolated ridge like a dot) or no ridges, could be generated at the ridge decision points. However, we excluded these types from ridge analyses due to their rarity in the experimentally fabricated patterns, compared to the other types.

To further study the structural organization, we simulated the generation of orthogonal patterns using two different algorithms with MATLAB by assuming that the ridge generation starts from the four corners of the structure and spreads to the center. First, when we assumed the determination of the ridge type was totally random (even probability for all ridge types), the results showed loop patterns (fig. S1B), which were hardly found in the fabricated physical structures (fig. S1A). This may be associated with the larger number of bifurcation in this probability model than that in the experiment (fig. S1D). Second, when we utilized the depth-first search (DFS) algorithm that is typically used for maze generation (fig. S1C), the pattern shape and the distribution of the ridge type were similar to the experiment. This resulted from the property of the DFS algorithm having a low branching factor. Overall, the ridge type seems to be determined with biased probability rather than being completely random. In addition, we guess that the pattern is determined like in the DFS algorithm with multiple starting points based on the sequence and directionality of the solvent evaporation and on the boundary effect of the structure.

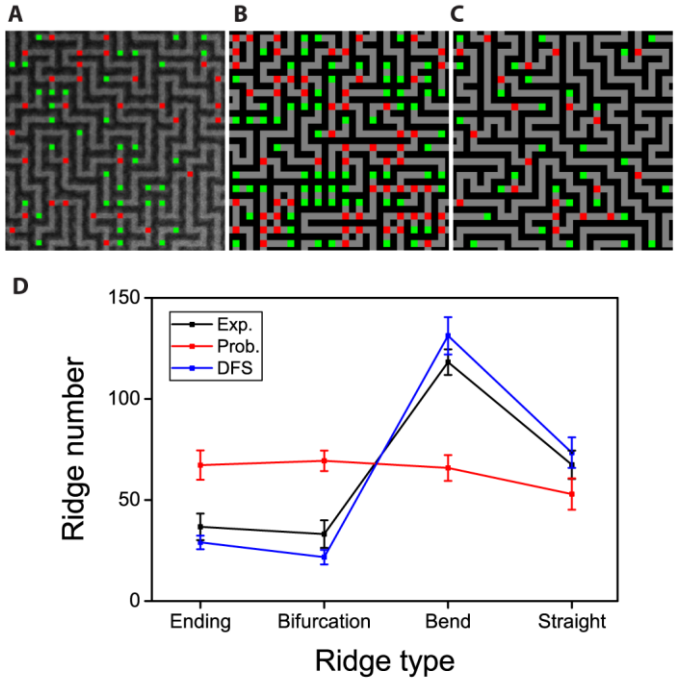

fig. S1. Comparative analysis of the orthogonal ridge pattern in different generation methods. (**A**) to (**C**) Representative ridge pattern obtained from the experiment (Exp.), probability-based model (Prob.), and depth-first search algorithm-based model (DFS), respectively. The green and red dots represent the ridge ending and bifurcation points, respectively. For data analysis, we extracted ridge information from the central areas of circular-shaped microparticles (25% of the particle) and standardized the extraction area to 16 × 16 lines in all groups. (**D**) Distribution of the ridge numbers according to the ridge type in each model. Each group contains ridge information from 20 patterns.

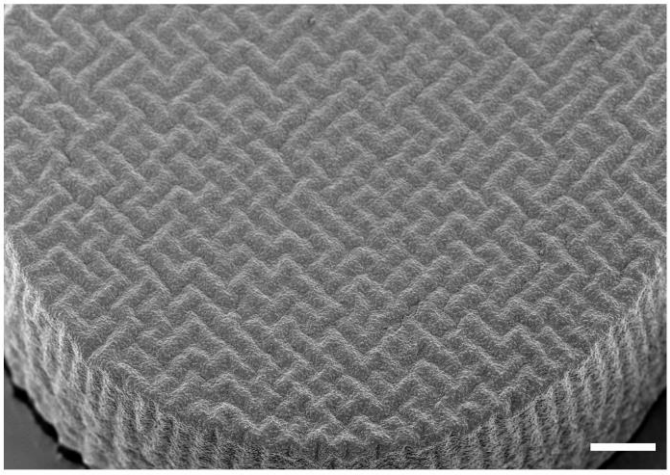

fig. S2. Scanning electron microscopy image of a maze microparticle (scale bar, 10 μm).

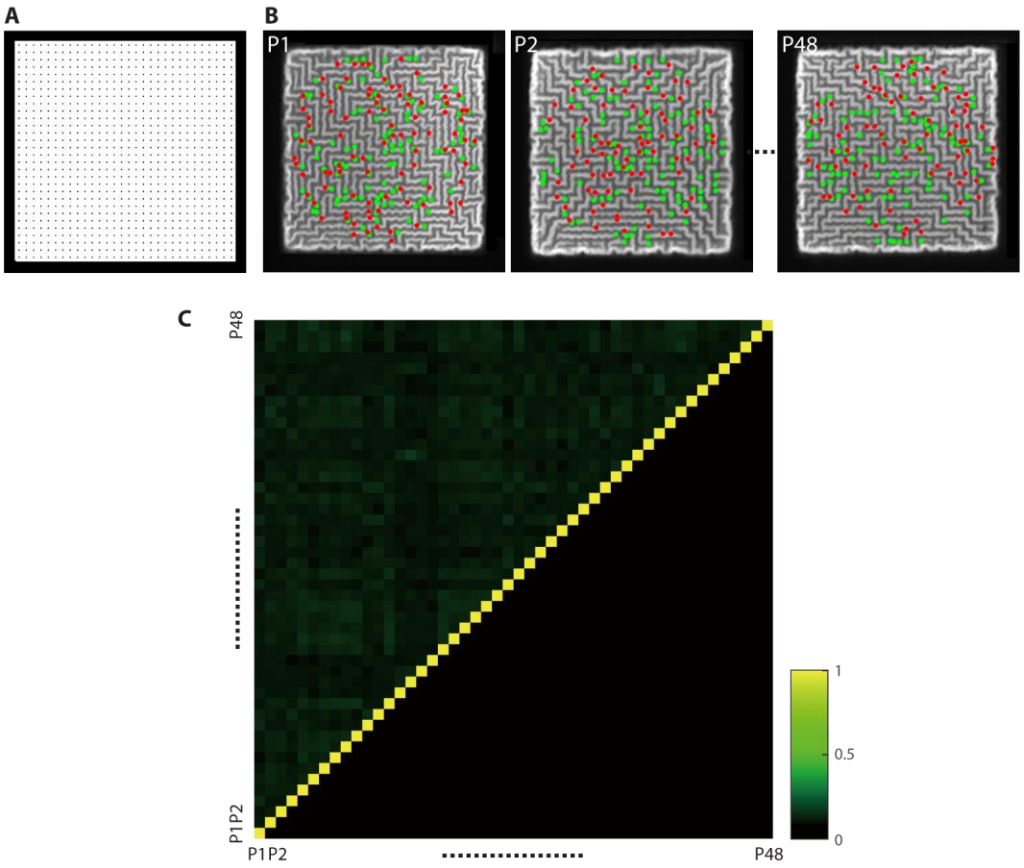

fig. S3. Uniqueness of orthogonal patterns. (**A**) A photomask design for the ridge guiding structure. (**B**) Extracted ridge information. The positions of ridge endings and bifurcations were extracted from the obtained CLSM images of each structure. This ridge distribution information was then stored in a 2D matrix (*36*). (**C**) Heat map of normalized cross-correlation values obtained from 48 orthogonal ridge patterns. The cross-correlation values between maze-like structures were calculated by performing a sliding inner-product of every combination of two matrices (*36*). A clear separation of higher intra-correlation values from lower inter-correlation values indicated that each maze transformed from the same prepatterned structure possessed a distinct pattern.

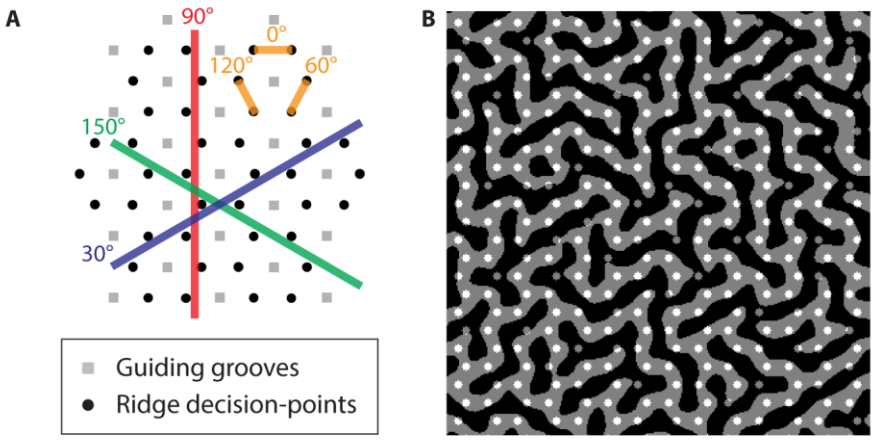

fig. S4. Ridge organization in a sigma tessellation. (**A**) A schematic diagram presenting possible ridge-guided lines and their angular orientations in the sigma tessellation. The ridge-guided lines with the angles of 0°, 60°, and 120° and those with the angles of 30°, 90°, and 150° can be observed microscopically and macroscopically, respectively. (**B**) A hexagonal ridge pattern image overlaid with the ridge decision points.

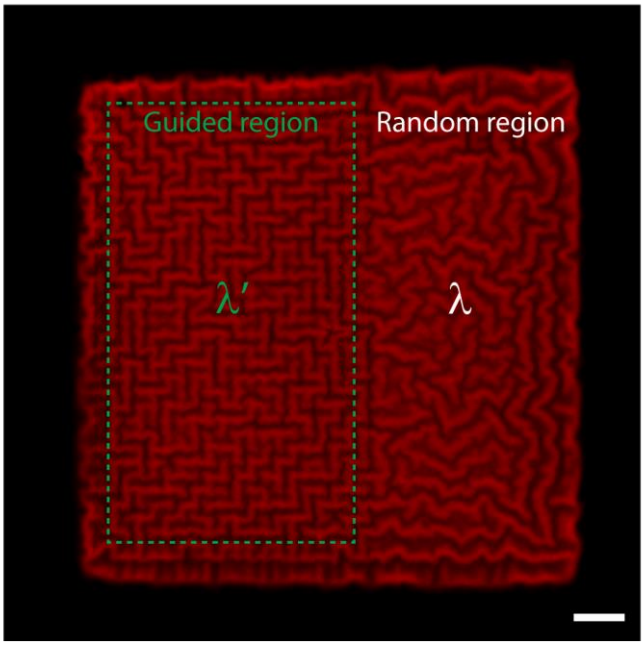

fig. S5. Microparticle design for studying the guiding effect. CLSM image of a wrinkled microparticle with both random and guided patterns. Scale bar, 10 μm. The characteristic wavelength (λ) and the constrained wavelength (λ′) were simultaneously extracted from the random and guided regions, respectively.

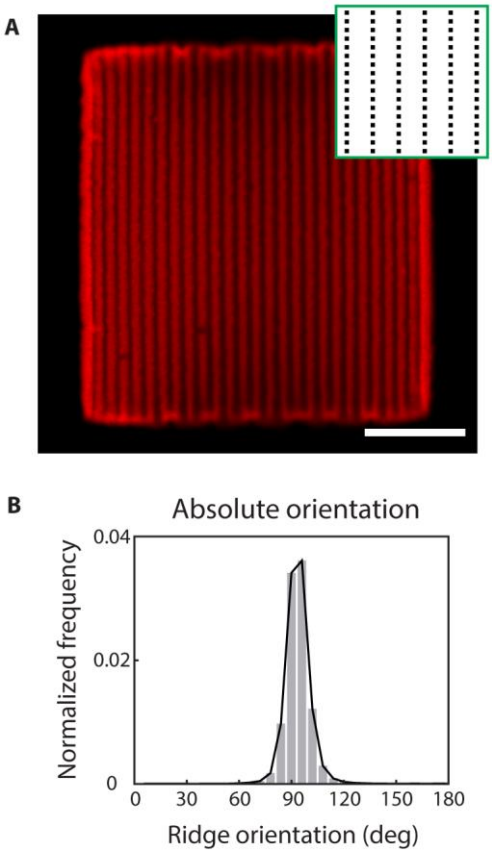

fig. S6. Controlling the anisotropic structure. (**A**) CLSM image of a unidirectionally ordered wrinkle pattern. The inset image shows a part of the photomask. Scale bar, 25 μm. (**B**) Distribution of the ridge orientation. The histogram contains ridge information from 20 microparticles.

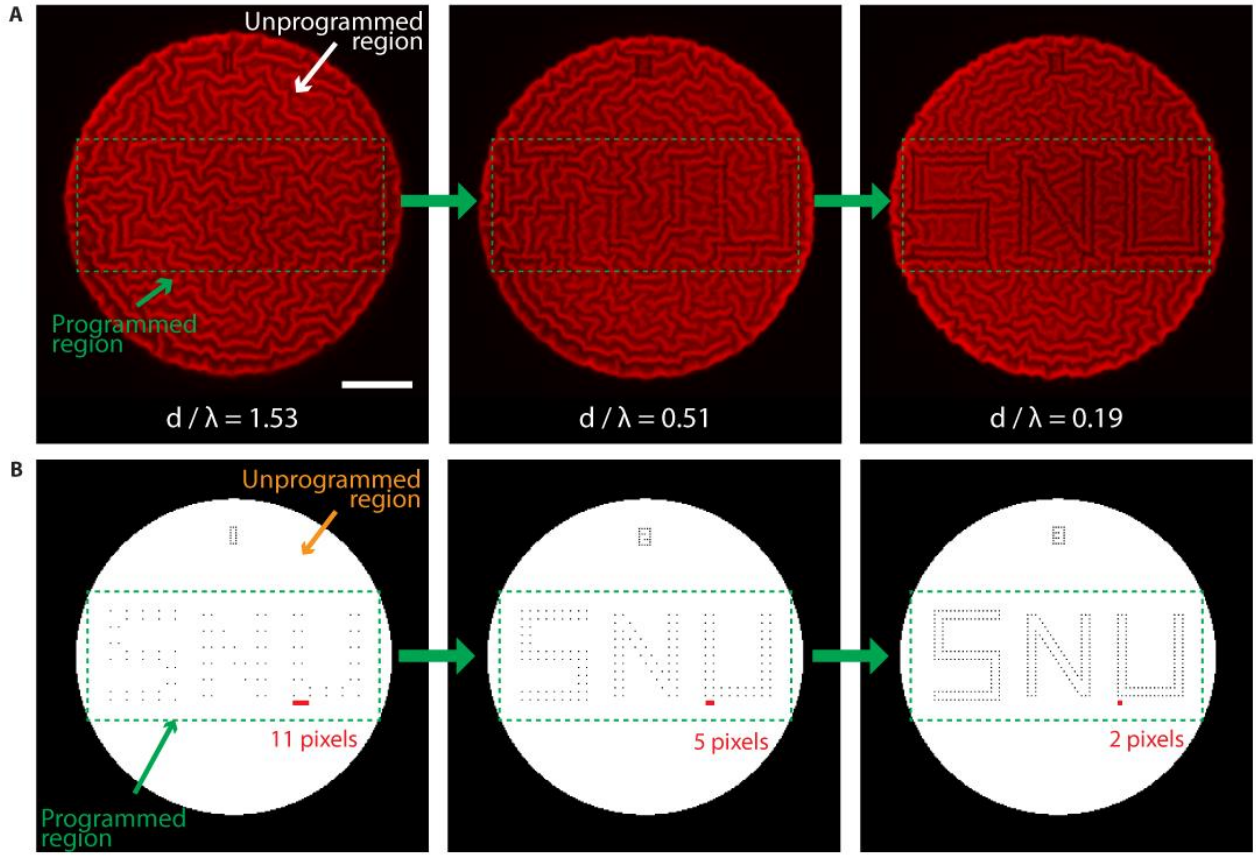

fig. S7. Inscribing letters with wrinkles. (**A**) CLSM images of wrinkled microparticles with programmed patterns. Scale bar, 25 μm. The programmed region showed letters, while the unprogrammed region presented random patterns. Letters in the programmed region became obvious as the d/λ values of the ridge-guiding structures decreased. (**B**) Photomask designs. The distances between dots for ridge-guiding grooves were 11, 5, and 2 pixels in the photomask, respectively.

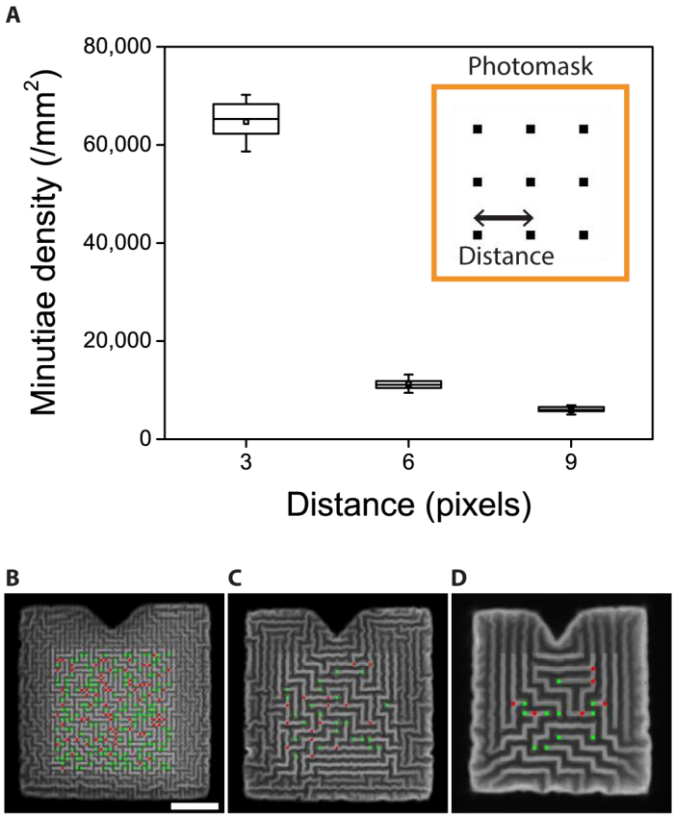

fig. S8. Control of the code complexity. (**A**) Boxplot showing minutiae density with different guiding structure dimensions. Center lines represent median values; white squares represent the average; box limits represent the interquartile range; whiskers range from the minimum to the maximum data point (n = 15 for each box). (**B**) to (**D**) Representative minutia patterns extracted from microparticle samples with different intergroove distances (3, 6 and 9, respectively). Scale bar, 25 μm. Green and red dots represent ridge endings and bifurcations, respectively.

movie S1. Generation of the guided wrinkles.